Angular momentum dependence of the GDR width in Sn nuclei at fixed excitation energy

M. Mattiuzzi [a], A. Bracco [a], F. Camera [a,1], W.E. Ormand [a,b],
J.J. Gaardhøje [c], A. Maj [c,d], B. Million [a], M. Pignanelli [a], T. Tveter [c,e]

[a] *Dipartimento di Fisica, Università degli Studi di Milano and Istituto Nazionale di Fisica Nucleare,*
Sezione di Milano, via Celoria 16, 20133 Milan, Italy
[b] *Physics Division, Oak Ridge National Laboratory, P.O. Box 2008, MS-6373, Oak Ridge, TN 37831-6373,*
USA
[c] *The Niels Bohr Institute, Blegdamsvej 15-17, Copenhagen DK-2100 Ø, Denmark*
[d] *Niewodniczański Institute of Nuclear Physics, Cracow, Poland*
[e] *Oslo University, Blindern, Norway*

Abstract

High-energy γ-rays from the decay of the giant-dipole resonance (GDR) in the hot ^{106}Sn compound nucleus and its daughters were measured in coincidence with heavy recoiling evaporation residues. The compound nucleus was formed at excitation energy $E^* = 80$ MeV using the reaction ^{56}Ni+^{48}Ti at a bombarding energy of 260 MeV. The analysis yields the GDR width for two different intervals of angular momentum $\langle J \rangle = 24$ and $36\hbar$. The present data, combined with previous data at higher angular momentum permit a study of the angular momentum dependence of the GDR width for $10 \leqslant J \leqslant 60\hbar$ at approximately fixed temperature. The width of the GDR is found to be roughly constant for $J < 35\hbar$, increasing rapidly for higher angular momenta. The data are found to be in good agreement with theoretical calculations within an adiabatic model describing thermal fluctuations of the nuclear shape. The model also reproduces the much weaker angular momentum dependence of the GDR width in the heavier nucleus ^{176}W.

---

[1] Permanent address: Polo didattico e di Ricerca di Crema, Università di Milano, Crema, Italy.

1. Introduction

The giant-dipole resonance (GDR) built on excited states has been extensively studied to obtain information on the properties of nuclei at high temperatures [1]. One of the central questions addressed by these studies is the understanding of the relaxation mechanisms of this collective mode. The width of the giant-dipole resonance in nuclei at finite temperature and angular momentum arises from collisional damping and from deformation changes of the nucleus. While the collisional damping width has been found to be approximately independent of temperature [2,3], shape effects arising from the coupling of the dipole vibration to the nuclear quadrupole deformation are very important, and are expected to depend on temperature and angular momentum [4,5]. At finite temperature the nucleus is characterized by an ensemble of deformations. Due to thermal fluctuations the giant dipole resonance couples to the different shapes whose probabilities are determined by the Boltzmann factor.

Several studies of the γ-decay of the giant-dipole resonance in hot, rotating nuclei have focused on the influence of shape fluctuations on the GDR line shape [1]. Most of the existing work was made employing heavy-ion fusion reactions in different mass ranges. By using different bombarding energies and projectile and target combinations, data associated with different temperatures and angular momenta were obtained and compared with the predictions of thermal fluctuation models [4,5].

Thus far, the most systematic study of the GDR cross section based on excited states has been made with Sn isotopes formed by heavy-ion fusion reactions [6–9]. These data show that the GDR width increases up to $\Gamma_{GDR} \approx 11$ MeV when the excitation energy increases up to ≈ 130 MeV. This increase was interpreted as arising from a change of the nuclear shape deformation induced by the combined effects of temperature and angular momentum. In order to provide a more stringent test for the model of thermal fluctuations the two effects must be separated. For example, by determining the dependence of the GDR cross section function on angular momentum (temperature) at fixed temperature (angular momentum).

More recently, two new GDR studies on excited Sn isotopes were made. One is based on a fusion–evaporation experiment in which the ^{108,110}Sn compound nuclei were formed at $E^* = 80$, 92 MeV and where the GDR width and angular distribution were studied as a function of angular momentum at approximately constant temperature [8]. An increase of the width and of the absolute value of the angular distribution of the a_2 coefficient was found for high angular momenta (40–54$\hbar$). The width increased from 10.8 to 12.8 MeV in that interval of angular momentum. The second study utilizes inelastic scattering of α particles on ^{120}Sn, which for small scattering angles leads to compound nuclei with angular momenta in the range from 5 to 20$\hbar$ [9]. In this study the GDR width was also found to increase as a function of temperature, from ≈ 5 MeV at $T \approx 1$ MeV ($E^* = 35$ MeV) to ≈ 12 MeV at $T \approx 3$ MeV ($E^* = 125$ MeV).

A possible explanation for the results of these two experiments is that at low angular momentum the GDR width is controlled by temperature-induced effects, while, at high angular momentum the GDR width is controlled by angular momentum effects. It seems

that at a given temperature, angular momentum effects begin to be important only above a certain value. The experimental confirmation of this hypothesis requires data on the GDR width in the angular momentum interval between the values explored by inelastic scattering and those explored by the fusion reaction experiment [8] in which angular momenta $J \geqslant 40\hbar$ were investigated.

The present paper reports on a measurement of the GDR width in ^{106}Sn at $E^* = 80$ MeV ($T \approx 2$ MeV) and for average spin values of 24 and 36$\hbar$. These results, together with those of the other existing exclusive measurements in the same excitation energy and mass region [8,9], permit a study of the angular momentum dependence of the GDR width, Γ_{GDR}, at fixed temperature. The set of Γ_{GDR} from ^{106}Sn with $E^* \approx 80$ MeV shows constancy of the Γ_{GDR} up to $J \approx 35\hbar$, after which value the GDR width increases significantly (see Section 4). This finding can be understood within the context of theoretical models of the GDR in hot nuclei that account for large-amplitude, thermal fluctuations of the nuclear shape. With the same model the temperature dependence of the GDR width at approximately zero momentum was calculated [16] and found in very good agreement with the inelastic scattering data [9].

The present analysis supports the concept that shape effects induced by angular momentum are mostly responsible for the measured angular momentum dependence of the GDR width once the temperature (E^*) is kept constant. In addition, a better understanding of the role of shape effects is obtained by comparing the results concerning the $A \approx 110$ mass region at $T \approx 1.8$ MeV with those for the much heavier nucleus ^{176}W at $T \approx 1.5$ MeV. In the latter case, the GDR width was measured as a function of angular momentum and found to be essentially constant, in good agreement with the results of model calculations.

2. The experimental method

The experiment was performed at the Tandem Laboratory of the Niels Bohr Institute. A 1 mg/cm^2 target of ^{48}Ti was bombarded by a beam of ^{58}Ni with kinetic energy of 260 MeV produced by the Tandem+Booster accelerator system. The detection system used, shown in Fig. 1, was the detector array HECTOR and two parallel-plate avalanche counters (PPAC) positioned at 44 cm from the target center. With this apparatus, it was possible to measure the energy and time of flight of high-energy γ-rays, the multiplicity and sum energy of low-energy γ-transitions, and the time of flight of the fused recoiling reaction products. The HECTOR array consists of 8 large volume BaF$_2$ crystals positioned at angles ($\pm 60°$, $\pm 90°$, $\pm 120°$, and $\pm 160°$) and 38 smaller BaF$_2$ detectors used as multiplicity filter. Neutron and γ separation was obtained by measuring the time of flight from the target. Gain shifts were monitored to better than 0.2% using an LED system optically coupled to the large BaF$_2$ crystals by optic fibers, and corrected off-line as necessary. The energy calibration of the high-energy detectors was done using the 15.1 MeV γ-rays from D(^{11}B,nγ)^{12}C* reaction as a high-energy point and utilizing the zero suppression mode of the ADC. A more complete description of HECTOR is
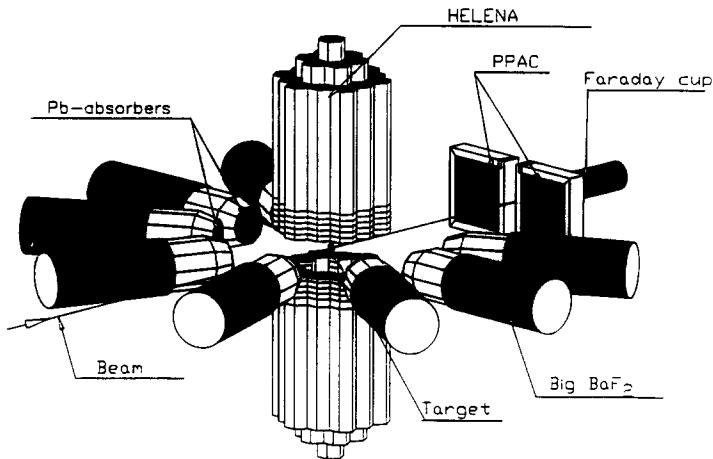
Fig. 1. Layout of the HECTOR-HELENA BaF$_2$ detector array operated in coincidence with 2 position-sensitive PPAC detectors for detection of fusion residues. The large volume BaF$_2$ detectors are used to measure γ-rays with $E_\gamma > 5$ MeV. The 38 element HELENA multiplicity filter is used as a time zero trigger and to select the rotational angular momentum.

given in Ref. [11].

The response function of the multiplicity filter was determined by making use of the method described in Ref. [12]. An absolute efficiency of 70% was measured for the 1.173 MeV line from a ^{60}Co source. The electronic threshold of the detectors was set at around 250 keV and the measured cross-talk between two elements was 12%.

The PPAC's detectors, each have an active area of 22 cm × 15 cm and were located at 44 cm from the target, covering the angular interval between 2.6° and 28° for the angle θ relative to the beam direction in the horizontal plane and ±9° for the ϕ angle relative to the vertical plane.

The geometrical efficiency of the setup was ≈ 10%. This number is the ratio of events consisting of high-energy γ-rays ($E_\gamma > 6$ MeV) in coincidence with a heavy evaporation residue and two or more low-energy γ-transitions with events for which the detection of heavy particles with the PPAC's was not required.

In Fig. 2, the time of flight spectrum, measured with the PPAC relative to the multiplicity filter for the reaction ^{58}Ni ($E_{beam} = 260$ MeV) + ^{48}Ti , is shown. This spectrum was obtained requiring a coincidence with high-energy γ-rays ($E_\gamma > 6$ MeV) and with at least one low-energy γ-ray. The random coincidences in this time of flight spectrum are characterized by several small peaks. These small peaks are due to the fact that the booster post accelerator system bunches the beam every 9.8 ns and that second harmonics are present in the cavity. Two strong and well separated peaks are present: the narrower corresponding to the detection of beam-like particles (denoted by (B) in Fig. 2), while the broader corresponds to recoiling evaporation residues (denoted by (F) in Fig. 2). The beam-like particles producing the (B) peak originate from many different types of reactions such as Coulomb excitation, deep inelastic, particle transfer, etc. The time difference between the two main intense peaks is ≈ 12 ns, in good agree-
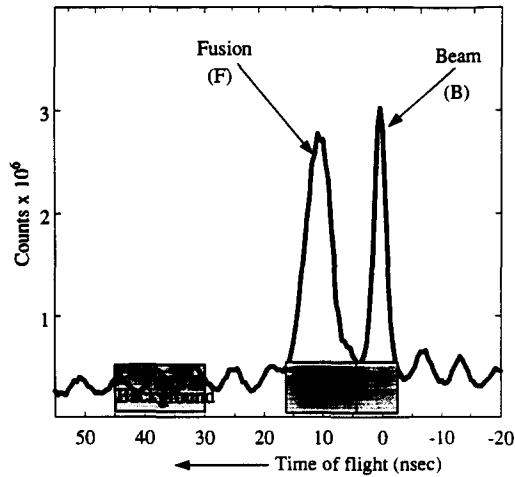
Fig. 2. The time of flight spectrum in the PPAC's of the heavy particles from the reaction ^{58}Ni + ^{48}Ti at beam energy 260 MeV. The two peaks correspond to fusion reactions (F), and to more peripheral reactions (B).

ment with the kinematics for the two types of reactions. The evaporation residues have a velocity $v_R = 1.6$ cm/s, which corresponds, in our case, to a transit time $t_R = 28$ ns, while the beam has a velocity $v_B = 2.9$ cm/ns with a transit time $t_B = 15$ ns. We have further identified the peak of the recoiling residues by changing the distance of the target to the PPAC.

The positive identification of the fusion channel by detection of heavy-recoiling residues has allowed one to study the GDR originating from compound nuclei at low angular momenta. In principle, compound nuclei with low angular momenta could be selected by choosing events with low multiplicity of low-energy γ-transitions. However, also other reactions with sizable cross sections, different than fusion, are characterized by a low multiplicity of γ-rays. The importance of requiring explicit fusion coincidence is exhibited in the top part of Fig. 3, where the fold distribution measured requiring coincidence with fusion residues (dot–dashed line) is compared with the inclusive fold distribution (shown with the dotted line). Here and in the following we define as multiplicity M_γ the number of low-energy γ-rays emitted in the reaction and with fold F_γ the number of coincident low-energy γ-rays that are detected in the multiplicity filter. Requiring coincidence with the recoiling residues in the PPAC, the measured fold distribution has a shape that is approximately triangular, as expected in the case of fusion reaction.

The measured coincidence fold distribution of low-energy γ-transitions in coincidence with heavy recoiling residues and with high-energy γ-rays is shown in the middle part of Fig. 3 (solid line) together with that obtained without the requirement of high-energy γ-rays. As expected, the maximum of the fold distribution in coincidence with high-energy γ-rays is slightly shifted down because the emission of high-energy γ-rays is
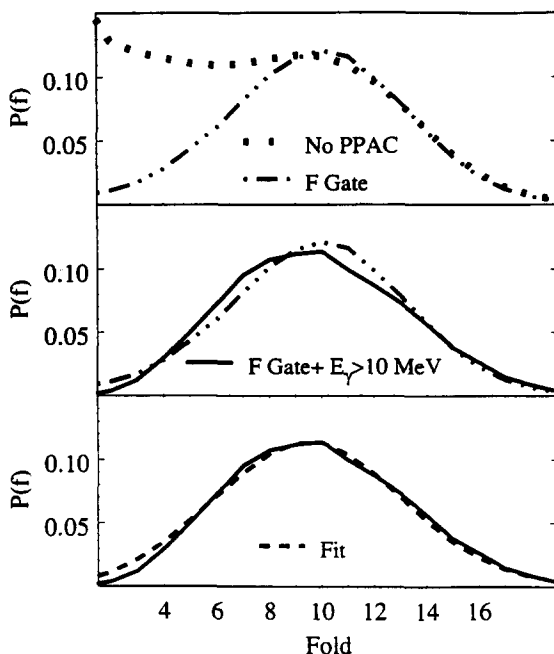
Fig. 3. Top panel: The dot–dashed line shows the coincidence fold distribution measured with the multiplicity filter for the present reaction ^{58}Ni + ^{48}Ti at E_{beam} = 260 MeV in coincidence with evaporation residues detected with the PPAC's. It is compared with the coincidence fold distribution measured without requiring coincidence with the PPAC's, shown with the dotted line. Middle panel: The coincidence fold distribution of the top panel is compared to the coincidence fold distribution that has the additional requirement of being in coincidence with a γ-ray with energy larger than 10 MeV (solid line). Bottom panel: The measured coincidence fold distribution is shown in comparison with the distribution obtained making use of the measured response of the filter and assuming that the fusion cross section has the shape described in the text (dashed line, here called fit).

larger at lower angular momentum (higher E^*).

The spectrum of high-energy γ-rays measured in coincidence with evaporation residues is shown in Fig. 4 with the solid line. It is obtained as a difference between the spectrum gated by heavy particles with time of flight in the region of the fusion peak and the spectrum associated with time of flight of the background region (see Fig. 2). In the same figure the spectrum of high-energy γ-rays in coincidence with beam-like particles (gated by (B)) is shown with the dotted line. The two spectra are normalized to the same channel width for the two different cases. Note that the two spectra differ not only for $E_\gamma > 10$ MeV, but also have different slopes at lower E_γ. The spectrum gated by (B) cannot be analyzed in detail since the reaction mechanism is not identified, hence also the excitation energy, the angular momentum, the nucleus mass and atomic numbers are not known. From this figure it is clear that if the fusion channel is not identified mistakes could be made in the interpretation of the gamma spectrum, particularly in the region below 10 MeV. This low-energy region is particularly interesting for the study of pre-equilibrium effects in fusion reactions. In fact, the latter should give
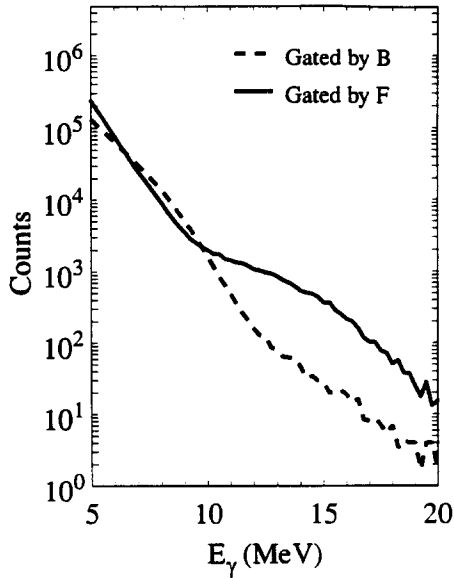
Fig. 4. Spectra of the high-energy γ-rays measured in coincidence with fusion evaporation residues (full drawn line) and with projectile like particles (dashed line) using ^{58}Ni + ^{48}Ti at E_{beam} = 260 MeV. The first spectrum is the result of gating by the (F) peak of Fig. 2 and the second results from gating on the (B) peak.

rise to γ-emission from very deformed nuclei, which should peak at $E_\gamma \approx 8$ MeV, but are expected to contribute to measured spectra for compound nuclei at higher excitation energy than that of the present study. In fact, the possible presence of pre-equilibrium effects was for the first time pointed out in the work of Ref. [7], presenting data at $E^* > 300$ MeV also obtained by explicit reaction channel selection. The present data emphasize the need for explicit reaction channel selection when discussing the E_γ = 8–12 MeV region. This selection is in many cases obtained in a more efficient way with a multiplicity filter alone (cf. for example Refs. [8,10,11]). In this work PPAC's detectors were also used because we wanted to study the low angular momentum region of the fusion cross section.

3. Experimental data analysis

High-energy γ-ray data discussed here have been selected by requiring a fusion event in the PPAC and by gating on different coincidence folds of low-energy transitions. Because of the limited accumulated statistics only two fold intervals, one from 3 to 6 and the other from 7 to 20 were considered.

The conversion between the measured coincidence fold F_γ (the number of measured coincident gamma rays of low energy in one event) to the multiplicity M_γ (the number of γ-rays emitted in the reaction) was established using the response matrix $S(M_\gamma, F_\gamma)$. The latter was obtained with the method described in [12] and making use of measurements with radioactive sources. It was also assumed that the multiplicity distribution
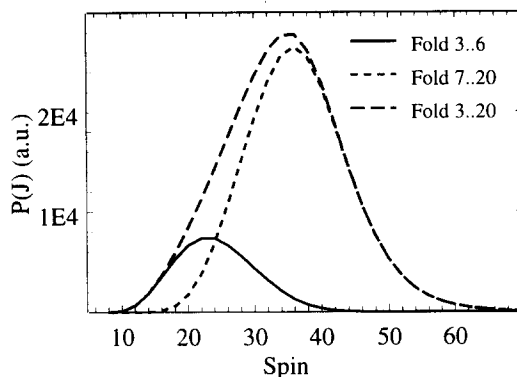
Fig. 5. The total distribution of the compound nucleus angular momentum, deduced from the measured coincidence fold, is shown together with the distributions corresponding to the coincidence fold intervals 3–6 and 7–20. These selected fold intervals are those associated to the data shown in Figs. 6 and 7.

following fusion reactions is given by $f(M_\gamma) = M_\gamma/(1 + \exp[(M_\gamma - M_0)/a])$. The maximum of the multiplicity M_0 and the diffuseness a were obtained by fitting to the expressions $\sum S(M_\gamma, F_\gamma) f(M_\gamma) = f_{\exp}(F_\gamma)$ where $f_{\exp}(F_\gamma)$ is the measured multiplicity spectrum in the region $1 < F_\gamma < 20$. The multiplicity distribution associated with each fold is $P(M_\gamma) = S(M_\gamma, F_\gamma) f(M_\gamma)$, with $M_0 = 23$ and $a = 2$ as it results from the fit. The FWHM of $P(M_\gamma)$ for each fold is ≈ 8. In the bottom part of Fig. 3 the fitting fold distribution (dashed line) is compared to the measurement of the same quantity.

The conversion from multiplicity to angular momentum was done assuming $J = 2M_\gamma + K$. In this expression, $K = 6$ takes into account the angular momentum removed by statistical γ-rays, particle emission and by the γ-rays below the trigger threshold [10]. In Fig. 5 we show the obtained total distribution of the compound nucleus angular momentum. It is plotted together with the distributions corresponding to the selected coincidence fold intervals, namely 3–6 and 7–20.

The measured γ-ray spectra associated with the selected angular momentum intervals were fit in the GDR region, namely from 8 to 18 MeV, with a modified version of the code CASCADE [13]. The centroid and the width values were obtained from the best fit to the data using a χ^2 minimization procedure. Because of the exponential nature of the spectra, the χ^2 of this fit is dominated by the low-energy part and relatively insensitive to the GDR region, consequently the best fit GDR parameters were chosen to be those minimizing the χ^2 divided by the number of counts. The used expression was $\chi^2 = \sum_i N_c(i)^{-1}[(N_c(i) - \text{Th}(i))^2/\sigma(i)^2]$, where $N_c(i)$ and $\text{Th}(i)$ denote the experimental and calculated values and $\sigma(i)^2$ the error in the spectrum channel i. For the fusion cross section as a function of angular momentum, the distribution deduced from the fold measurements was used as input to the statistical model calculations. The error of the GDR parameters include the statistical error and the uncertainties related to the spin assignment and to the incident energy.

The data associated to selected regions of the coincidence fold spectrum are shown
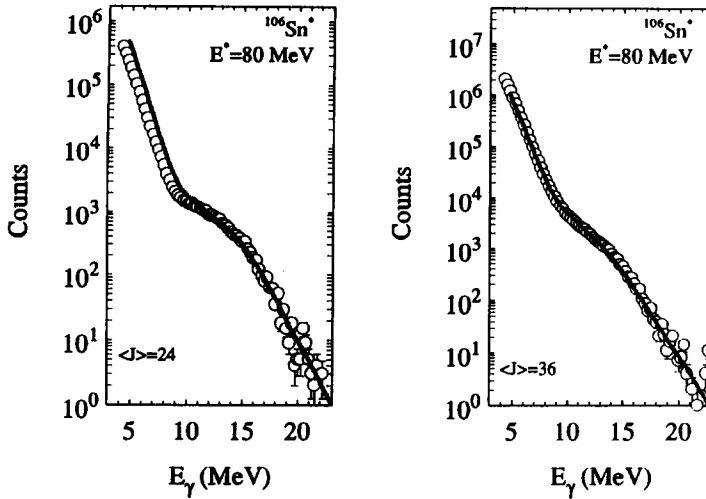
Fig. 6. Experimental spectra for ^{106}Sn at $E^* = 80$ MeV associated to average spin values $24\hbar$ (left panel) and $36\hbar$ (right panel). Superimposed to the data are the best fitting statistical model calculations.

in Fig. 6 together with the statistical model calculations. In the region $E_\gamma < 8$ MeV, dominated by γ-decay below the nucleon binding energy, the data for $\langle J \rangle = 24\hbar$ are not equally well reproduced as those for $\langle J \rangle = 36\hbar$. Since the discrepancy occurs only in one case it is difficult to understand it, particularly in terms of background subtraction. Discrepancies in the same region were seen in data at much larger excitation energy ($E^* > 300$ MeV) also obtained with the explicit detection of the reaction channel [7]. In contrast to the present case, an excess over the calculation was found. However, the extraction of the GDR parameters for compound nuclei in this mass region is basically unaffected by the quality of the fit at $E_\gamma < 8$ MeV.

In order to display spectra on a linear scale to emphasize the GDR region, the quantity

$$F(E_\gamma) * Y_\gamma^{\text{exp}}(E_\gamma)/Y_\gamma^{\text{cal}}(E_\gamma)$$

associated to the data points was plotted in Fig. 7. $Y_\gamma^{\text{exp}}(E_\gamma)$ is the experimental spectrum and $Y_\gamma^{\text{cal}}(E_\gamma)$ the best fit calculated spectrum, corresponding to the Lorentzian function $F(E_\gamma)$ that describes the GDR in the fitting process. The Lorentzian functions $F(E_\gamma)$ are also shown in Fig. 7 with the solid lines.

The results of the statistical model analysis are $E_{\text{GDR}} = 15.8 \pm 0.5$ MeV and $\Gamma_{\text{GDR}} = 8.5 \pm 1$ MeV in the case of average angular momentum $\langle J \rangle = 24\hbar$ and $E_{\text{GDR}} = 15.4 \pm 0.5$ MeV and $\Gamma_{\text{GDR}} = 9.6 \pm 1$ MeV in the case of average angular momentum $\langle J \rangle = 36\hbar$. Both the centroid and the width are found to be rather constant for the two angular momentum values. To discuss the damping mechanisms of the giant dipole resonance at finite temperature the values of the width obtained with the statistical model analysis of the present γ-ray spectra are compared with the existing data and to the model predictions in the next section.
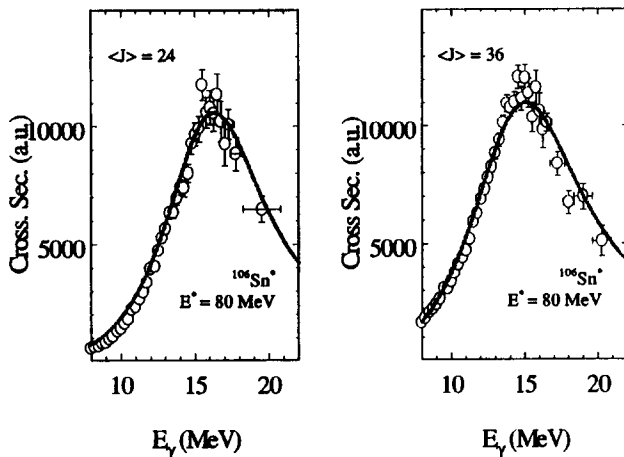
Fig. 7. The measured strength functions of ^{106}Sn at the two angular momentum intervals centered at 24 (left) and 36 (right) $\hbar$. In the figure the quantity $F(E_\gamma) * Y_\gamma^{exp}(E_\gamma)/Y_\gamma^{cal}(E_\gamma)$ (see text) is plotted for the data points. The full drawn lines correspond to the best fitting single component Lorentzian functions. The values of the measured GDR parameters are $E_{GDR} = 15.8$ MeV, $\Gamma_{GDR} = 8.5$ MeV for $\langle J \rangle = 24\hbar$ and $E_{GDR} = 15.4$ MeV, $\Gamma_{GDR} = 9.6$ MeV for $\langle J \rangle = 36\hbar$.

4. Experimental results and comparison with theory

The measured GDR widths from the present experiment are compared in the bottom part of Fig. 8 with the existing systematics for reactions leading to similar compound nuclei at approximately the same excitation energy but at different values of rotational angular momentum. In the figure, the horizontal bars indicate the FWHM of the angular momentum distribution associated with the selected coincidence fold interval. As one can see from the figure, the GDR width (denoted in that figure by Γ_{FWHM}), which we define as the full-width at half-maximum (FWHM) of the GDR Lorentzian, is fairly constant up to an angular momentum of approximately $35\hbar$, but increases rapidly with increasing angular momentum above this value.

To understand this behavior, we recall the important influence of quadrupole deformation on the GDR line shape. In particular, we note that the energy of the GDR modes are inversely proportional to the length of the nuclear principal axes. Therefore, for a given deformation, defined by the parameters β and γ, the GDR is composed of three components with centroid energies given by [14]

$$E_k = E_0 \frac{R_0}{R_k} = E_0 \exp\left[-\sqrt{\frac{5}{4\pi}}\beta \cos\left(\gamma + \frac{2}{3}\pi k\right) \right], \qquad (1)$$

where $E_0 \approx 80A^{-1/3}$ MeV is the energy of the GDR associated with the spherical shape. It is further important to note that at finite excitation energy, the nucleus does not possess a single determined shape, but rather explores a broad ensemble of shapes due to thermal fluctuations. At a temperature, $T \neq 0$, the probability of any given quadrupole

shape and orientation (defined relative to an external reference frame by the three Euler angles ψ, θ, and ϕ) is governed by the Boltzmann factor, i.e.,

$$P(\beta, \gamma, \phi, \theta, \psi; T) \propto \exp\left[\frac{-F}{T}\right], \tag{2}$$

where F is the nuclear free energy, which is a function of the deformation parameters, Euler angles, angular momentum, and temperature of the compound nucleus.

Under the assumption that the time scale associated with thermal fluctuations of the nuclear shape is long compared with the shift, ΔE_{GDR}, caused by the fluctuations, i.e., the adiabatic limit, the GDR cross section is made up as a weighted average over all shapes and orientations. Projecting angular momentum, J, the GDR cross section is evaluated via [15,16]

$$\sigma(E) = Z_J^{-1} \int \frac{\mathcal{D}[\alpha]}{\mathcal{I}(\beta, \gamma, \theta, \psi)^{3/2}} \sigma(\alpha, \omega_J; E) \exp\left(-F(T, \alpha, J)/T\right), \tag{3}$$

where α denotes the deformation and orientation parameters, E is the photon energy,

$$\mathcal{D}[\alpha] = \beta^4 \, d\beta \sin(3\gamma) \, d\gamma \sin\theta \, d\theta \, d\phi \, d\psi$$

is the volume element, and

$$Z_J = \int \mathcal{D}[\alpha] / \mathcal{I}^{3/2} e^{-F/T}.$$

The free energy is given by

$$F(T, \boldsymbol{\alpha}, J) = F(T, \boldsymbol{\alpha}, \omega_{\rm rot} = 0) + (J + \tfrac{1}{2})^2 / 2\mathcal{I}(\beta, \gamma, \theta, \psi), \tag{4}$$

where $F(T, \boldsymbol{\alpha}, \omega_{\rm rot} = 0)$ is the free energy evaluated in the cranking approximation with rotational frequency, $\omega_{\rm rot}$, equal to zero, and the factor $\mathcal{I}(\beta, \gamma, \theta, \psi)$ is given by

$$\mathcal{I}(\beta, \gamma, \theta, \psi) = I_1 \cos^2\psi \sin^2\theta + I_2 \sin^2\psi \sin^2\theta + I_3 \cos^2\theta, \tag{5}$$

where the I_k represent the deformation-dependent principal moments of inertia.

The nuclear free energies were computed using the standard Nilsson–Strutinsky [17] procedure extended to finite temperature [18] using the Nilsson and liquid-drop parameters of Refs. [19,20], respectively. For the most part, the shell corrections for ^{106}Sn were found to be quite small, and for all practical purposes can be ignored. In addition, shell corrections to the moments of inertia were also evaluated, and found to be negligible. As such, the moments of inertia were taken to correspond to the rigid-body values with radius $R = r_0 A^{1/3}$, $r_0 = 1.2$ fm.

Here, as in many previous studies [15,21,22], the GDR is modeled with a rotating, three-dimensional harmonic oscillator. Within this context, the GDR is composed of three fundamental modes whose energies are given by Eq. (1). Including the Coriolis term, the Hamiltonian for the GDR in the intrinsic frame may be written as [23]

$$H_D = \sum_k \tfrac{1}{2}(p_k^2 + E_k^2 d_k^2) - \boldsymbol{\omega}_{\rm rot} \cdot (\boldsymbol{d} \times \boldsymbol{p}), \tag{6}$$

where d_k and p_k are the coordinates and conjugate momenta associated with the dipole vibration and ω_{rot} is the rotational frequency, which is chosen to be aligned along the z-axis in the external reference frame. In addition, ω_{rot} is taken to be the saddle-point frequency $\omega_J = (J + \frac{1}{2})/\mathcal{I}(\beta, \gamma, \theta, \psi)$, i.e., the rotational frequency that maximizes the exponential factor while projecting angular momentum onto the partition function (see Refs. [15,16]). The GDR cross section in the intrinsic frame is evaluated with the three eigenstates $|\nu\rangle$ of H_D, and may be written as

$$\sigma^{int}(\alpha, \omega_J; E) = \sigma_0 \sum_{\mu,\nu} |\langle \nu | d_\mu | 0\rangle|^2 E[\mathrm{BW}(E, E_\nu, \Gamma_\nu) - \mathrm{BW}(E, -E_\nu, \Gamma_\nu)],$$

(7)

where $\sigma_0 = (4\pi^2 e^2 \hbar/3mc)(2ZN/A)$, d_μ is the dipole coordinate written in terms of spherical components, $\mathrm{BW}(E, E', \Gamma) = \Gamma/[2\pi((E - E')^2 + \Gamma^2/4)]$, and Γ_ν is the intrinsic damping width for the resonance. In keeping with experimental findings [24], Γ_ν depends on the centroid energy E_ν via $\Gamma_\nu = \Gamma_0(E_\nu/E_0)^\delta$, where Γ_0 is the width for the spherical shape and $\delta \approx 1.8$. The laboratory cross section for each deformation and orientation used in Eq. (3) is evaluated by rotating the matrix elements $\langle \nu | d_\mu | 0\rangle$ from the intrinsic frame to the fixed external reference frame and by shifting the dipole energies associated with the intrinsic μ components by $-\mu\omega_{rot}$ [23]. Note that in the limit $\omega_{rot} = 0$, the GDR cross section is a sum of three normalized Lorentzians with centroids $E_\nu^C = \sqrt{E_\nu^2 + \Gamma_\nu^2/4}$ and width Γ_ν satisfying 100% of the classical sum rule. Finally, the parameters E_0 and Γ_0 were taken from ground-state data and for ^{106}Sn are $E_0 = 15.0$ MeV and $\Gamma_0 = 5.0$ MeV.

From Eq. (1) it is clear that thermal averaging, as dictated by Eq. (3), will, in general, lead to an overall broadening of the GDR, as the temperature of the compound nuclear system increases. This is primarily brought about because, at finite temperature, the nucleus experiences a wide range of deformations that individually contribute three lines with centroids given by Eq. (1). In addition, because of the β^4 factor in the volume element $\mathcal{D}[\alpha]$, the mean value of β, defined as

$$\langle \beta \rangle = Z^{-1} \int \frac{\mathcal{D}[\alpha]}{\mathcal{I}^{3/2}} \beta \exp(-F/T),$$

(8)

is non-zero even for nuclei whose free energies have a minimum at $\beta = 0$, such as in ^{106}Sn. Therefore, as a function of temperature, the principal mechanism behind the increase in the FWHM of the GDR strength function is a splitting of the individual (and often unresolved) components of the GDR due to an increasing $\langle \beta \rangle$.

With increasing angular momentum, the nucleus tends to undergo oblate flattening due to centrifugal effects. This is characterized by a shift in the minimum of the nuclear free energy to oblate non-collective shapes ($\gamma = 60°$), whose magnitude is determined by the interplay between the surface and rotational energies, and is sensitive to the moment of inertia of the system. Because of the dependence in the free energy on the inverse of the moment of inertia, one finds that for lighter nuclei, such as ^{106}Sn, the equilibrium deformation, β_{eq}, increases rapidly with angular momentum, and as a consequence, the
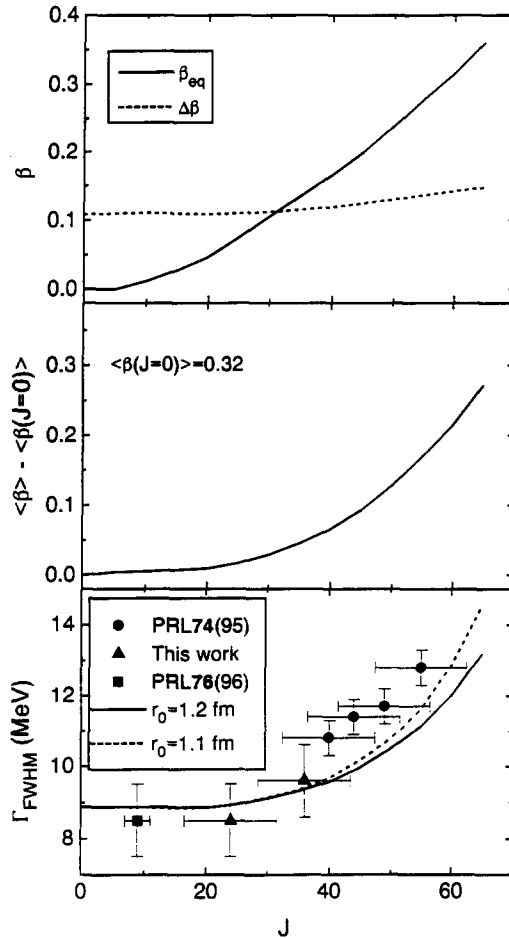
Fig. 8. Top panel: Evolution of the equilibrium deformation (full drawn line) for ^{106}Sn at $T = 1.8$ MeV as a function of the angular momentum $\langle J \rangle$. The dashed line shows the value of $\Delta\beta$ defined in the text. Middle panel: The mean nuclear deformation with respect to that at zero angular momentum is shown. Bottom panel: The measured values of the GDR width from this work (filled triangles) and those from previous works are compared with predictions of the thermal fluctuation model. The horizontal bars represent the full-width half-maximum of the spin distribution associated to the experimental data. Two assumptions were made for the moment of inertia of the nucleus, one that is equal to that of a rigid rotor (full drawn line), and the other that is 16% smaller (dashed line).

total GDR strength function undergoes a further splitting, which increases the FWHM. It should be pointed out, however, that even though the equilibrium deformation increases with angular momentum, an increase in the FWHM of the GDR does not occur until the equilibrium deformation increases sufficiently to affect the value of $\langle \beta \rangle$. It should also be noted that in addition to the mean value, the nucleus also experiences a spread in deformations, which can be measured by the variance $\Delta\beta = \sqrt{\langle \beta^2 \rangle - \langle \beta \rangle^2}$. While $\beta_{eq} < \Delta\beta$, the mean deformation $\langle \beta \rangle$ does not increase significantly, and, as such, neither does the FWHM. For the most part, at low angular momentum, the effect of the

equilibrium deformation is "washed out" by the thermal fluctuations. This is illustrated in the top panel of Fig. 8, where, for ^{106}Sn, β_{eq} is compared with the variance $\Delta\beta$. The increase in the mean value of β as a function of angular momentum is shown in the middle panel of Fig. 8.

In the bottom panel of Fig. 8, the FWHM values obtained from theoretical calculations for ^{106}Sn at $T = 1.8$ MeV using Eq. (3) are compared with experimental data (solid line). For the most part, theory and data are in overall agreement. In particular, the constancy of the GDR-FWHM up to angular momentum $J \sim 35\hbar$ is well reproduced. Indeed, by comparing the middle and bottom panels, a clear correlation between the FWHM and $\langle\beta\rangle$ is seen. At higher angular momenta, the theoretical values appear to be systematically smaller than the experimental values. It should be pointed out however, that the results of the data are somewhat sensitive to the choice of the level-density parameter a, and as such the extracted temperatures are uncertain by a few hundred keV. In addition, the experimental data were obtained by fitting to a single Lorentzian, while the theoretical cross sections comprise a sum of several Lorentzians. A further supposition may lie in the moment of inertia being somewhat smaller than the rigid-body values. As such, we repeated the calculation while setting the radius parameter $r_0 = 1.1$ fm (dotted line), which represents a 16% reduction in the moment of inertia. We find that the FWHM is increased slightly at higher values of angular momentum, in better agreement with experiment.

Following the arguments outlined above regarding the angular momentum dependence of the FWHM, it should then be expected that for heavier nuclei, such as ^{176}W or ^{208}Pb, the effect of oblate flattening should be reduced. As a consequence the FWHM should exhibit less dependence on angular momentum. This is clearly exhibited in the top panel of Fig. 9, where the experimental FWHM for ^{176}W at $T \approx 1.5$ MeV (obtained from Ref. [25]) is seen to be essentially constant as a function of angular momentum. This is also in overall agreement with theoretical predictions, as is illustrated by the dashed line in the figure.

To further illustrate the influence of the moment of inertia on the FWHM of the GDR as a function of angular momentum, we compare (in the bottom panel of Fig. 9) the FWHM for the nuclei ^{106}Sn, ^{120}Sn, ^{176}W, and ^{208}Pb as a function of angular momentum at temperatures of the order 1.5–1.8 MeV. In the figure, it is seen that the dramatic increase in the FWHM on angular momentum exhibited by ^{106}Sn is significantly abated in the heavier nuclei. Indeed, in ^{120}Sn, which, with its 14 additional neutrons, has a moment of inertia that is approximately 15% smaller than ^{106}Sn, the increase in the FWHM at $60\hbar$ is nearly 2 MeV smaller. Again, the correlation with the increase in the mean value of β, which is shown in the middle panel of Fig. 9 for each of the nuclei, is evident.
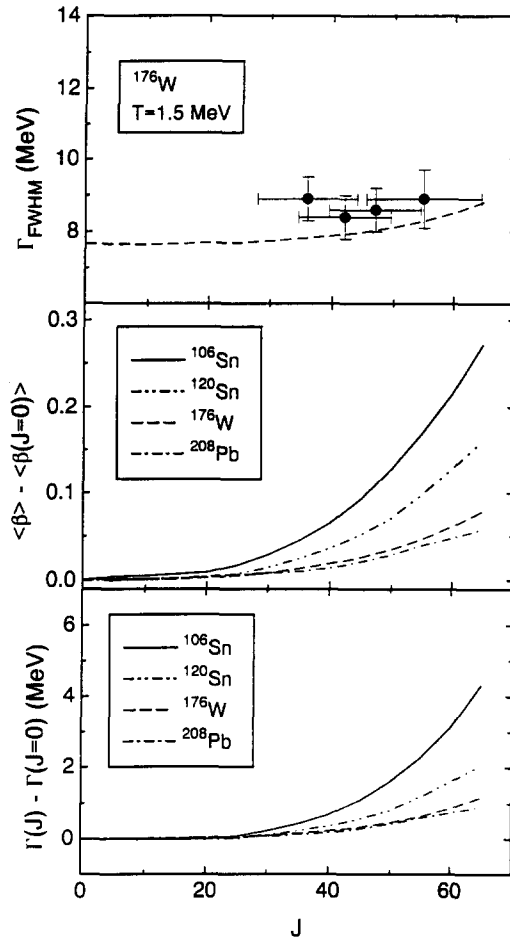
Fig. 9. Top panel: Evolution of the width of the giant dipole resonance in ^{176}W at $T = 1.5$ MeV. The data points are compared with the predictions of the thermal fluctuation model described in the text. The horizontal bars represent the full-width half-maximum of the spin distribution associated to the experimental data. Middle panel: The mean nuclear deformation with respect to that at zero angular momentum for different nuclei (for Sn isotopes $T = 1.8$ MeV while for ^{176}W and ^{208}Pb $T = 1.5$ MeV.) Bottom panel: Evolution of the GDR width with angular momentum as predicted by the thermal fluctuation model. The plotted values are relative to zero angular momentum and are given for different nuclei.

5. Summary and conclusions

In summary, this paper presents a systematic study of the width of the giant-dipole resonance in excited Sn isotopes as a function of angular momentum at fixed temperature. The study is based on the results of a new measurement of the high-energy γ-rays emitted by hot compound nuclei formed with the reaction ^{58}Ni ($E_{\text{beam}} = 260$ MeV) + ^{48}Ti and on other existing *exclusive* data. With the experimental set up used in this work, data were collected by detecting high-energy γ-rays in coincidence with a multiplicity filter

and the heavy recoiling residual nuclei.

At an average temperature of approximately 1.8 MeV the width of the GDR observed in ^{106}Sn is found to be essentially constant up to $\approx 35\hbar$. Above this value it increases rapidly with angular momentum. This dependence on angular momentum is also exhibited in the results of theoretical calculations that include the effects of thermal fluctuations of the nuclear shape and orientation on the GDR line shape. For the most part, the FWHM of the GDR is found to be governed by the mean value of the quadrupole deformation, which increases with angular momentum because of oblate flattening. Calculations of the same type at ≈ 0 angular momentum also reproduce the temperature dependence of the GDR width [9,16].

The Sn data are also compared with those obtained from the heavier nucleus ^{176}W, where the FWHM of the GDR is found to be essentially constant as a function of angular momentum. This behavior is also explained within the context of the theoretical model, where the increase in the mean quadrupole deformation is found to be roughly proportional to the inverse of the moment of inertia. As a consequence, the magnitude of the oblate flattening is considerably reduced in the heavier nuclei, which leads to a much smaller increase in the FWHM with increasing angular momentum.

It is possible to summarize by saying that at the moderate temperatures considered here, namely $T = 1.5$ and $T = 1.8$ MeV, the influence of the rotational angular momentum on the GDR width is strongly dependent on the nuclear moment of inertia. As a consequence, angular momentum effects are important above $40\hbar$ for the $A = 110$ mass region, but unimportant for the heavier ^{176}W nucleus. It would be interesting to extend these studies to lighter nuclei where a more dramatic dependence on angular momentum is expected.

Acknowledgements

References

[1] J.J. Gaardhøje, Annu. Rev. Nucl. Part. Sci. 42 (1992) 483, and references therein.
[2] P.F. Bortignon et al., Nucl. Phys. A 460 (1986) 149.
[3] F.V. De Blasio et al., Phys. Rev. Lett. 68 (1992) 1663;
    B. Lauritzen et al., Phys. Rev. Lett. 74 (1995) 5190;
    P. Donati, N. Giovanardi, P.F. Bortignon and R.A. Broglia, to be published in Phys. Lett. B.
[4] W.E. Ormand et al., Phys. Rev. Lett. 64 (1990) 2254; 69 (1992) 2905.
[5] Y. Alhassid and B. Bush, Phys. Rev. Lett. 65 (1990) 2527; Nucl. Phys. A 514 (1990) 434; A 531 (1991) 1.

[6] J.J. Gaardhøje et al., Phys. Rev. Lett. 56 (1986) 1783;
    D.R. Chakrabarty et al., Phys. Rev. C 36 (1987) 1886;
    A. Bracco et al., Phys. Rev. Lett. 62 (1989) 2080.
[7] J.H. Le Faou et al., Phys. Rev. Lett. 72 (1994) 3321.
[8] A. Bracco et al., Phys. Rev. Lett. 74 (1995) 3748.
[9] E. Ramakrishnan et al., Phys. Rev. Lett. 76 (1996) 2025.
[10] F. Camera et al., Phys. Lett. B 293 (1992) 18.
[11] A. Maj et al., Nucl. Phys. A 571 (1994) 185.
[12] M. Jäskelainen et al., Nucl. Instr. Meth. 204 (1983) 385.
[13] F. Puhlhofer, Nucl. Phys. A 280 (1977) 267.
[14] A. Bohr and B.R. Mottelson, Nuclear Structure, Vol. 2 (Benjamin, New York, 1975).
[15] Y. Alhassid and N. Whelan, Nucl. Phys. A 565 (1993) 427.
[16] W.E. Ormand, P.F. Bortignon and R.A. Broglia, Phys. Rev. Lett. 77 (1996) 607.
[17] V.M. Strutinsky, Yad. Fiz. 3 (1966) 614 [Sov. J. Nucl. Phys. 3 (1966) 449]; Ark. Fys. 36 (1966) 629;
    Nucl. Phys. A 95 (1967) 420; A 122 (1968) 1.
[18] M. Brack and P. Quentin, Nucl. Phys. A 361 (1981) 35.
[19] S.G. Nilsson et al., Nucl. Phys. A 131 (1969) 1.
[20] C. Guet et al., Phys. Lett. B 205 (1988) 427.
[21] M. Gallardo et al., Nucl. Phys. A 443 (1985) 415;
    J.M. Pacheco, C. Yannouleas and R.A. Broglia, Phys. Rev. Lett. 61 (1988) 294;
    Y. Alhassid and B. Bush, Nucl. Phys. A 509 (1990) 461;
    Y. Alhassid, B. Bush and S. Levit, Phys. Rev. Lett. 61 (1988) 1926.
[22] B. Lauritzen et al., Phys. Lett. B 207 (1988) 238;
    Y. Alhassid and B. Bush, Phys. Rev. Lett. 63 (1989) 2452.
[23] K. Neergård, Phys. Lett. B 110 (1982) 7.
[24] P. Carlos et al., Nucl. Phys. A 219 (1974) 61.
[25] M. Mattiuzzi et al., Phys. Lett. B 364 (1995) 13.